



Kinetic study and the effect of particle size on low temperature CO oxidation over Pt/TiO₂ catalysts



Na Li^a, Qiu-Yan Chen^a, Liang-Feng Luo^b, Wei-Xin Huang^b, Meng-Fei Luo^a,
Geng-Shen Hu^a, Ji-Qing Lu^{a,*}

^a Key Laboratory of the Ministry of Education for Advanced Catalysis Materials, Institute of Physical Chemistry, Zhejiang Normal University, Jinhua 321004, China

^b Hefei National Laboratory for Physical Sciences at the Microscale and Department of Chemical Physics, University of Science and Technology of China, Hefei 230026, China

ARTICLE INFO

Article history:

Received 29 March 2013

Received in revised form 26 May 2013

Accepted 28 May 2013

Available online 4 June 2013

Keywords:

CO oxidation

Pt/TiO₂ catalysts

Particle size effect

Kinetic study

Pt–TiO₂ interface

ABSTRACT

A series of Pt/TiO₂ catalysts with various Pt particle sizes were prepared and tested for low temperature CO oxidation. The effect of Pt particle sizes on the reaction was investigated. It was found that turnover frequencies based on Pt dispersion varied as declined with increasing Pt particle size as a function of $d^{-0.86}$. However, turnover frequency based on Pt atoms located on the periphery of Pt–TiO₂ interface remained constant at 40 °C, implying that these periphery Pt atoms were the active sites. Kinetic study was conducted to investigate reaction pathway on the catalyst. The derived power rate law expression was $r = 1.98 \times 10^{-7} P_{CO}^{0.29} P_{O_2}^{0.19}$ at 40 °C. Based on the kinetic results, elementary steps of this reaction were proposed, which involved chemisorption of CO on Pt atoms and chemisorption of O₂ on TiO₂ and a reaction of these two species at the Pt–TiO₂ interface.

© 2013 Elsevier B.V. All rights reserved.

1. Introduction

Catalytic oxidation of CO is of great importance because of its wide applications in such as indoor air cleaning, CO gas sensors, CO₂ lasers, automotive exhaust treatment [1,2]. The catalyst systems for CO oxidation consist of precious metals such as Au [3,4], Pt [5–7], and Pd [8] and transition metals such as Cu [9,10]. Although supported Au catalysts recently have been paid much attention because of their extraordinary activities at low temperatures, Pt catalysts are also promising for this reaction, especially when Pt is supported on reducible oxides such as TiO₂ [11] or FeO_x [12].

CO oxidation is also a good model reaction to understand some essential questions in catalysis, such as structure–sensitivity (particle size effect), active sites/phases and reaction mechanism. Concerning the particle size effect, it is generally accepted that the supported Pt catalysts show less structure sensitivity or structure insensitivity [13] for the CO oxidation compared to the Au catalysts, and sometimes the turnover frequency (TOF) decreases with increasing Pt dispersion [14]. In addition, the particle size effect is also dependent on the reaction model. Most commonly, the particle effect is established according to the relationship between the

metal particle size and the turnover frequency (TOF) for CO oxidation based on metal dispersion. Such a correlation is true when all the surface metal atoms participate in the reaction; however, when metals are supported on reducible oxides such as TiO₂, Fe₂O₃ and CeO₂, it is accepted that CO oxidation takes place at the metal–support interface [15]. In this case, only the metal atoms located at the periphery of metal–support interface are the reacting sites while the other surface metal atoms serve as collection zone, thus the relation between the TOF concerning periphery metal atoms and metal particle diameter seems reflect more intrinsic size dependency. For example, we have recently studied the particle size effect on CO oxidation over CuO–CeO₂ catalysts [16]. It was found that according to the turnover frequency based on CuO sites located on the CuO–CeO₂ interface, the activity on a large CuO crystallite was much higher than that on the small one. The enhanced activity was ascribed to a higher density of chemisorbed CO on the active sites for the large CuO crystallite.

The mechanism of CO oxidation over Pt catalysts has been extensively studied in literature and various reaction pathways were proposed [17–21]. It is generally recognized that the reaction occurs on the Pt surface and the reaction follows Langmuir–Hinshelwood (L–H) models [22–24], which involves chemisorption of CO and O₂ on the Pt surface. Note such reaction pathways were derived on Pt supported on inert oxides such as Al₂O₃ [25]. When metal is supported on reducible oxides such as TiO₂ and CeO₂, the mechanism

* Corresponding author. Tel.: +86 579 82287325; fax: +86 579 82282595.

E-mail addresses: gshu@zjnu.edu.cn (G.-S. Hu), jiqinglu@zjnu.cn (J.-Q. Lu).

may change since the support could also participate in the reaction via the involvement of lattice oxygen, which has been widely reported. For example, Behm and co-workers [26] concluded that on Au/TiO₂ catalysts the active oxygen species are surface lattice oxygen (most likely at the perimeter of Au particles) and gas phase oxygen is not required in the CO oxidation. Thus, an “Au-assisted Mars-van Krevelen reaction mechanism” was proposed [27]. Unfortunately, detailed kinetic study was not performed in their works and the dependency of O₂ partial pressure on the reaction rate was not determined.

It can be seen that to better understand the particle size effect on CO oxidation, a series of carefully controlled catalysts should be prepared. Besides, appropriate deduction of TOF according to the reaction model is helpful to establish intrinsic correlation between activity and particle size. Moreover, detailed kinetic investigation is required to obtain some insight on the reaction mechanism, although mechanisms of CO oxidation over Pt catalysts have been proposed, reaction pathways of this reaction over Pt catalysts supported on reducible oxides has not been studied. Therefore, in this work, we prepared a series of Pt/TiO₂ catalysts with different Pt loadings. By using Pt(NO₃)₂ as the precursor instead of H₂PtCl₆, and calcination under same temperature, catalysts with different Pt particle sizes were obtained without changing any other parameters. These catalysts were tested for CO oxidation in order to clarify the particle size effect. In addition, kinetic investigation was also performed to discuss reaction mechanism on these catalysts.

2. Experimental

2.1. Catalyst preparation

A series of Pt/TiO₂ catalysts with different Pt loadings were prepared using an incipient wetness method. In a typical synthesis procedure, an appropriate amount of aqueous solution of Pt(NO₃)₂ (Shanghai Jiuyue Chemical Ltd., 99.9%) was added to 5 g of TiO₂ support (P25, Degussa, 55 m² g⁻¹, calcined at 500 °C for 4 h prior to catalyst preparation), and the mixture was kept for 3 h. Then it was mildly evaporated at 90 °C and dried at 120 °C overnight. Finally, the solid was calcined at 400 °C for 4 h. The catalysts were designated as xPt/TiO₂, as the x referred to the weight percent of Pt in the catalyst. A reference catalyst Pt/SiO₂ with a Pt loading of 2.0 wt.% was also prepared in a similar manner.

2.2. Catalyst characterizations

X-ray diffraction (XRD) patterns were recorded using a PANalytic X'Pert PW3040 diffractometer with Cu K α radiation operating at 40 kV and 40 mA. The patterns were collected in a 2 θ range from 10° to 90°, with a scanning step of 0.15°/s.

High-resolution transmission electron microscopy (HRTEM) was performed on a JEM-2100F microscopy with a field emissive gun, operated at 200 kV and with a point resolution of 0.24 nm. The samples were prepared by dispersing a few milligrams of powder in ethanol. The dispersion was then immersed for 10 min in an ultrasonic bath in order to disagglomerate the powder particles. Finally, one drop was deposited on a Formvar/carbon copper grid. Various regions of the grid were observed and the particle sizes were measured from the observation of 6–20 particles.

CO chemisorption experiments were carried out on a Quantachrome CHEMBET-3000 instrument in order to determine the dispersion of Pt. The Pt/TiO₂ catalyst was placed in a U-shaped quartz reactor and a high-purity He (99.999%) gas flow of 70 ml min⁻¹ was used as the carrier gas. Before CO chemisorption, the samples were reduced in a H₂-N₂ mixture (5 vol% H₂) stream at 300 °C for 1 h, cooled down to 30 °C, and then purged with a

pure He gas flow (30 ml min⁻¹) for 1 h at the same temperature. Then pulses of CO were fed into the stream of carrier gas with a precision analytical syringe.

The reduction properties of the samples were measured by hydrogen temperature-programmed reduction (H₂-TPR) experiments. The Pt/TiO₂ catalyst was placed in a quartz reactor, and then heated from room temperature to 800 °C at a rate of 10 °C min⁻¹ in a H₂-N₂ gas (5 vol% H₂, 30 ml min⁻¹). The hydrogen consumption during the reduction was determined by a gas chromatograph with a thermal conductivity detector (TCD). The water produced in TPR was trapped on a 5 Å molecular sieve.

X-ray photoelectron spectra (XPS) were recorded using a VG ESCALAB MK-2 spectrometer with Al K α radiation (1486.6 eV). The voltage and power for the measurements were 12.5 kV and 250 W, respectively. The vacuum in the test chamber during the collection of spectra was kept at 2 \times 10⁻⁸ Pa. The spectra obtained, once the background was removed, were fitted to Lorentzian and Gaussian lines to obtain the number of components, peak position, and their areas. The adventitious C 1s line at 284.6 eV was used as an internal standard.

O₂ chemisorption over the Pt/TiO₂ catalysts were performed home-made apparatus. 0.1 g of the catalyst was loaded in the middle of a quartz tubular reactor attached with a thermal couple. The catalyst was pretreated in a Ar flow (30 ml min⁻¹) at 300 °C for 1 h to remove the water and some carbonates. Then the catalyst was cooled down to a certain temperature (e.g. 40, 60 or 80 °C), then a O₂-Ar mixture (10% O₂, total flow rate = 20 ml min⁻¹) was introduced to the sample. In the mean time, the outlet O₂ signal was monitored by a mass spectrometer (MS, Qic-20 Benchtop, Hiden Analytical) with a *m/e* = 32. When the O₂ chemisorption was saturated, the signal became constant. The amount of chemisorbed O₂ could be calculated based on the MS signal profile, as shown in Fig. 11 with the area of the shadow part representing the amount of chemisorbed O₂. In order to subtract the dead volume of the apparatus, a blank test was also conducted by loading the same volume of quartz sand as the catalyst.

Diffuse reflectance infrared Fourier transform (DRIFT) spectra of the samples were recorded using a Nicolet 670 spectrometer equipped with a MCT detector and a DRIFT cell (Harrick, CHC-CHA-3). Prior to the measurement, the sample was pretreated in a O₂-He flow (20% O₂, total flow = 30 ml min⁻¹) at 300 °C for 30 min to remove the water and some carbonate species on the catalyst surface. After that, the sample was cooled down to 40 °C and a flow of Ar (30 ml min⁻¹) was fed to remove the residual gas and the background spectrum was recorded. Then the sample was exposed to CO-Ar mixture (30 ml min⁻¹, 1 vol% CO) for 30 min. Finally, the sample was purged by Ar (30 ml min⁻¹) for another 30 min to remove the gaseous and physisorbed CO and the spectra were recorded. In all cases the spectra were taken at 30 °C, with a resolution of 4 cm⁻¹ and cumulative 32 scans. The temperature was controlled with a thermocouple in direct contact with the sample, and circulating water was used to cool the body of the cell. CO chemisorption experiments at 60, 80 and 100 °C were conducted in a similar way. Another set of experiments were carried out over a 2.0Pt/TiO₂ catalyst at elevated temperatures after CO chemisorption at 40 °C. After the catalyst was exposed in a CO-Ar mixture (30 ml min⁻¹, 1 vol% CO) for 30 min at 40 °C and purged by Ar (30 ml min⁻¹) for 30 min and a spectrum was recorded, the temperature was continuously raised to 60, 80 and 100 °C, then spectra were recorded again.

2.3. Catalytic testing

Catalytic CO oxidation was performed on a tubular quartz micro reactor (6 mm i.d.) using different amounts of catalyst

(0.12–0.15 mm in size). Different weight of the catalyst was employed in order to control the CO conversion at low levels (typically below 20% at low reaction temperatures (<100 °C) to ensure a differential reaction mode). The catalyst was diluted with quartz sand in the same mesh size to 0.25 ml. A feed gas consists of 1% CO and 1% O₂ in N₂ with a total flow rate of 40 ml (NTP) min⁻¹, corresponding to a space velocity (S.V.) of 9600 ml g_{cat}⁻¹ h⁻¹. The catalyst was directly exposed to reaction gas without any pretreatment. The reaction temperature was monitored by a thermocouple placed in the middle of the catalyst bed. The CO concentration in the reactor effluent was analyzed using an Agilent 6850 gas chromatograph equipped with a TCD detector attached to an HP PLOT column (30 m x 0.32 mm x 12 μm).

Concerning the intrinsic activity, two types of turnover frequencies (TOFs) were calculated based on the following definitions:

$$\text{TOF}_a (\text{s}^{-1}) = X_{\text{CO}} F_{\text{CO}} \frac{M_{\text{Pt}}}{m_{\text{Cat}} X_{\text{Pt}} D_{\text{Pt}}}$$

where X_{CO} is the CO conversion at certain temperature; F_{CO} is the flow rate of CO in unit of mol s⁻¹; m_{Cat} is the amount of catalyst; X_{Pt} is the Pt loading in the catalyst; D_{Pt} is the dispersion of Pt; M_{Pt} is the molar weight of Pt (195.08 g mol⁻¹). TOF_a reflects the conventional calculation of turnover frequency based on the metal dispersion.

$$\text{TOF}_b (\text{s}^{-1}) = X_{\text{CO}} F_{\text{CO}} N_{\text{AV}} \frac{m_{\text{Pt,c}}}{m_{\text{Cat}} X_{\text{Pt}}} \frac{1}{7.8\pi d}$$

where X_{CO} is the CO conversion at certain temperature; F_{CO} is the flow rate of CO in unit of mol s⁻¹; N_{AV} is the Avogadro's constant; m_{Cat} is the amount of catalyst; X_{Pt} is the Pt loading in the catalyst; $m_{\text{Pt,c}}$ means the weight of a single Pt crystallite depending on its size, which could be derived from its volume obtained under the assumption of its semi-spherical shape and density of Pt (14.9 g cm⁻³); d is the crystallite size of Pt; 7.8 is the average site density of Pt on the periphery, calculated by $\pi/2d_{(\text{Pt-Pt})}$, where $d_{(\text{Pt-Pt})}$ is the distance of Pt–Pt bond (0.202 nm). TOF_b reflects the turnover frequency based on the metal sites located on the Pt–TiO₂ interface.

2.4. Reaction kinetics

The kinetic study was performed on the same fixed bed reactor of the catalytic CO oxidation as mentioned above. The feed gases were measured with mass flow controllers and mixed prior to the reactor inlet. For kinetic measurements, the reactor was operated in a differential mode with CO conversion less than 15%. The reaction conversion was controlled by changing the load of catalyst, which was diluted with quartz sand to a volume of 0.1 ml. The diluted catalyst was embedded with glass wool on both sides. A thermocouple was inserted into the middle of the catalyst bed to monitor the reaction temperature. Also, the absence of mass transport resistances was also checked by Weisz–Prater criterion for internal diffusion and Mears' criterion for external diffusion and the absence of heat transfer was checked by Mears' criterion [28] (See Supplementary Information for detailed calculation). For the 2.0Pt/TiO₂ catalyst, the calculated values under kinetic conditions are 3.66 x 10⁻³ for the Weisz–Prater criterion for internal diffusion, 6.74 x 10⁻³ for the Mears' criterion for external diffusion and 0.10 for the Mears' criterion for heat transfer. Those results ensure plug-flow and isothermal conditions within the catalyst bed. Partial pressure dependencies of the reaction rates were measured by adjusting the flow rate of 10% CO/Ar or 10% O₂/Ar, while keeping the total flow rate at 120 ml min⁻¹ by adjusting the flow rate of pure Ar. In this kinetic experiment, the concentration of CO or O₂ in the feed was varied between 0.1 and 3%. Each measurement was taken after stable rate was achieved, which took about 1 h. CO₂ concentration in the outlet gas stream was also analyzed by the same

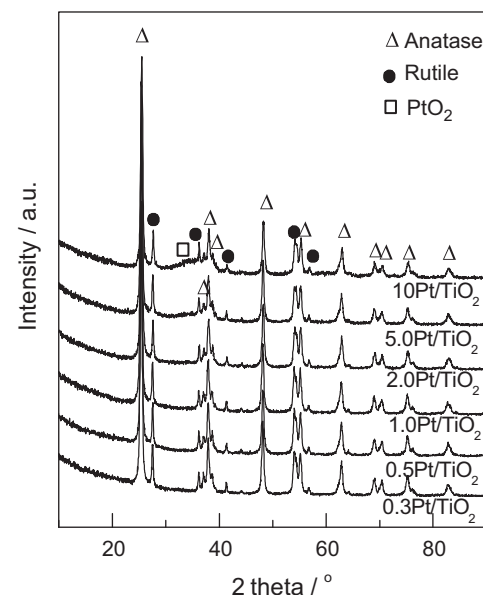


Fig. 1. XRD patterns of Pt/TiO₂ catalysts.

Agilent 6850 gas chromatograph mentioned above. Conversion of CO was calculated as follows:

$$X_{\text{CO}} = \frac{[\text{CO}]_{\text{in}} \text{ vol.\%} - [\text{CO}]_{\text{out}} \text{ vol.\%}}{[\text{CO}]_{\text{in}} \text{ vol.\%}}, \quad (1)$$

where $[\text{CO}]_{\text{in}}$ and $[\text{CO}]_{\text{out}}$ were the CO concentrations in the inlet and outlet gas (vol.%) respectively. And the X_{CO} was used to calculate the reaction rate as follows:

$$r_{\text{CO}} = \frac{N_{\text{CO}} \cdot X_{\text{CO}}}{W_{\text{cat}}}, \quad (2)$$

where N_{CO} is the CO molar gas flow rate in mol s⁻¹, W_{cat} is the catalyst weight in grams, r_{CO} is the reaction rate in mol_{CO} g_{cat}⁻¹ s⁻¹.

The power-rate law expressions were obtained by taking partial pressure of each reactant (kPa) and the reaction rate data and simultaneously fitting the entire data set by linear least squares regression analysis using the POLYMATH 5.1 program [29].

3. Results and discussion

3.1. Characterizations of Pt/TiO₂ catalysts

Fig. 1 presents the XRD patterns of the Pt/TiO₂ catalysts. All these catalysts show typical TiO₂ diffraction peaks in forms of anatase (PDF 21-1272) and rutile (PDF 21-1276). While for the high loading Pt catalysts, very weak diffraction peaks at $2\theta = 33.6^\circ$ due to PtO₂ (PDF 38-1355) could be observed.

Representative HRTEM images of the Pt/TiO₂ catalysts are shown in Fig. 2. It is clear that the particle size of Pt/PtO gradually increases with the metal loading in the catalyst. For the 0.3Pt/TiO₂ catalyst, the average particle size is about 1 nm, while for the 10Pt/TiO₂ catalyst the particle size is about 10 nm. These results are in good agreement with the CO chemisorption results (Table 2), indicating the growth of particles with increasing metal loading in the catalyst.

Analysis of the oxidation states of the Pt/TiO₂ catalysts were conducted by XPS, and the results are shown in Fig. 3. The Pt4f_{5/2} peaks of all the catalysts could be deconvoluted to three peaks at 71.3, 72.3 and 74.3 eV, which could be assigned to Pt⁰, Pt²⁺ and Pt⁴⁺, respectively [30–32]. It can be seen that the Pt species in these catalysts are predominantly oxidized, with very limited metallic Pt content (<3%). This is because the catalysts were calcined. Also,

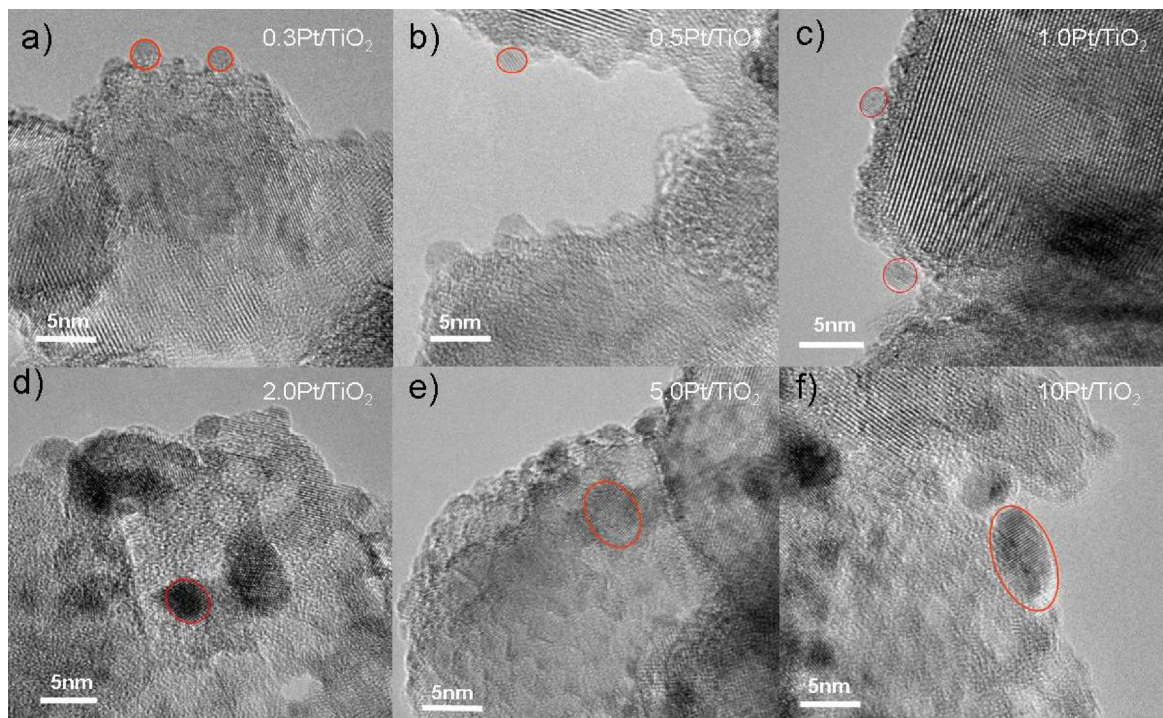


Fig. 2. TEM images of Pt/TiO₂ catalysts.

the peak intensity increases with the increase of Pt content in the catalyst.

Redox properties of the Pt/TiO₂ catalysts are measured by H₂-TPR technique, as shown in Fig. 4. A low-temperature reduction peak at about 100 °C and a high-temperature reduction peak in the range of 300–500 °C were observed. The peak at 100 °C could be assigned to the reduction of PtO_x [33], while the broad peak at 300–500 °C could be attributed to the reduction of TiO₂ caused by spillover effect [34]. However, note that the area of the low-temperature peak is not proportional to the metal loading in the catalyst and it is well known that PtO_x could be easily reduced even at room temperature [35], it implies that some PtO_x species

might be readily reduced at low temperature before the signal was recorded.

It seems clear that the as-prepared catalysts contain mostly oxidized Pt species in the catalysts. However, the oxidation states of the Pt species may change under reaction conditions, because the reaction feedstock consists of both CO (reducing agent) and O₂ (oxidizing agent). Fig. 5 shows the DRIFT spectra of CO chemisorption on the 2.0Pt/TiO₂ catalyst at different temperatures. It can be seen that the catalyst presents similar features of bands at 2064, 2098 and 2112 cm⁻¹, which could be assigned to CO chemisorbed on Pt⁰, Ptⁿ⁺ (1 < n < 2) and Pt²⁺, respectively [36–38]. Meanwhile, the peak intensity dramatically increases with temperature, suggesting

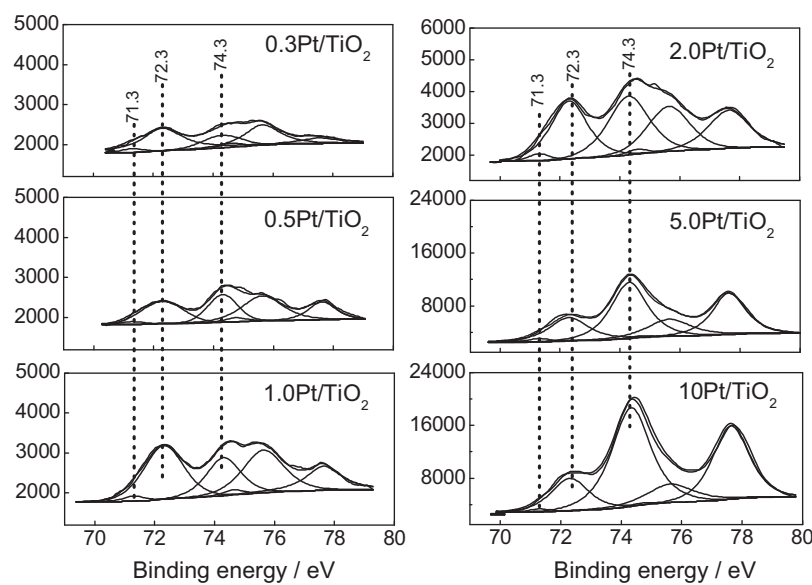
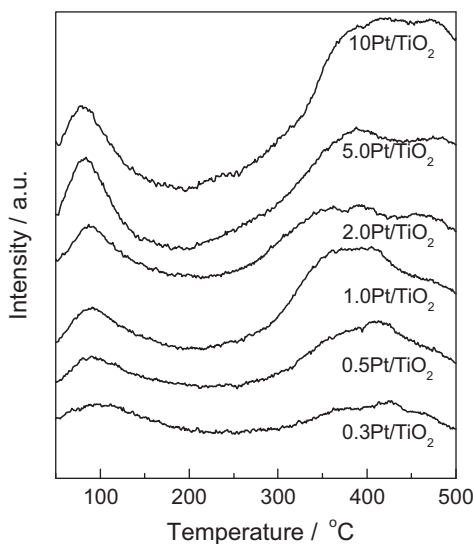
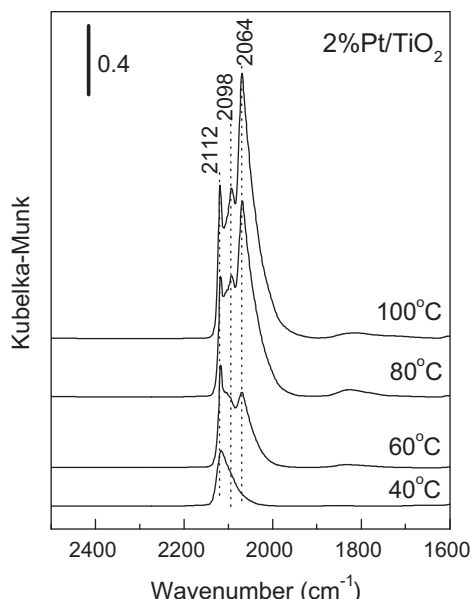
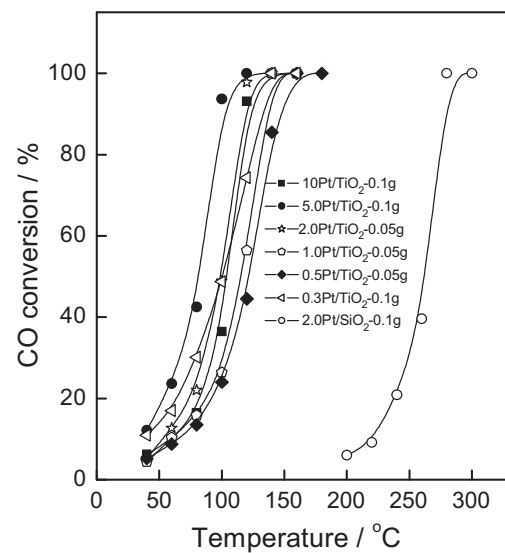


Fig. 3. Pt_{4f} XPS spectra of Pt/TiO₂ catalysts.

Fig. 4. H_2 -TPR profiles of Pt/TiO_2 catalysts.

stronger CO chemisorption on the catalyst at elevated temperature. Moreover, the disappearance of Pt^{4+} species after CO chemisorption implies the reduction of Pt^{4+} species by CO molecules. The reduction of oxidized Pt species was also evidenced by the changes of intensity of the bands. At 40 °C, the band at 2112 cm^{-1} (CO-Pt^{2+}) is dominant; while the bands at 2064 (CO-Pt^0) and 2098 (CO-Pt^{n+} ($n=1-2$)) increase in intensity at higher temperatures and become dominant at 100 °C. Meanwhile, the relative intensity of the band at 2112 cm^{-1} (defined as $I_{2112}/(I_{2064} + I_{2098} + I_{2112})$) declines continuously. These results suggest that the surface Pt species in oxidized forms could be easily reduced, which is in good agreement with the H_2 -TPR results (Fig. 4). Although the CO chemisorption experiments are not the same as the reaction conditions because of the absence of O_2 , it has been reported that the oxidized Pt species could be readily reduced under reaction conditions even with low CO concentration. For example, Gracia et al. [39] performed IR experiments on a calcined Pt/SiO_2 catalyst with a 1% CO and 10%

Fig. 5. DRIFT spectra of CO chemisorption on 2.0Pt/TiO₂ catalyst at different temperatures.Fig. 6. Light-off curves of CO oxidation over Pt/TiO_2 catalysts.

O_2 mixture, and they found that the oxidized Pt species could be reduced at 120 °C.

Thus, by changing the Pt loadings, catalysts with PtO_x sizes ranging from 1 to 10 nm were prepared. The as-prepared catalyst contains mostly oxidized Pt species, however, these species could be easily reduced in the presence of CO, and the catalyst contains a mixture of Pt^0 , Pt^{n+} ($n=1-2$) and Pt^{2+} under the reaction condition.

3.2. Activity test and the effect of Pt particle size

Fig. 6 demonstrates the activity tests of the Pt/TiO_2 catalysts. Note that in order to obtain low conversion levels (<20%) at temperature below 100 °C, different catalyst weights were used. For example, the catalyst loadings of the 0.5Pt/TiO₂, 1.0Pt/TiO₂ and 2.0Pt/TiO₂ were 0.05 g, while the loadings of the other catalysts were 0.1 g. Also, the 2.0Pt/SiO₂ catalyst is much less active than those supported on TiO₂, which catalyzes CO oxidation at about 200 °C. The enhancement of activity over the Pt/TiO₂ catalysts compared to the Pt/SiO₂ catalyst strongly confirms the participation of TiO₂ in the reaction. The CO conversions at 40 °C over the Pt/TiO₂ catalysts are summarized in Table 1, as well as the TOF values calculated based on Pt dispersion (TOF_a) or based on Pt atoms located on the periphery of Pt-TiO₂ interface. It can be seen that the TOF_a at different reaction temperatures declines with increasing Pt particle size by a factor of about 7. For example, at 40 °C, the TOF_a obtained on the 0.3Pt/TiO₂ was $21.5 \times 10^{-3} \text{ s}^{-1}$ while that on the 10Pt/TiO₂ catalyst was $3.2 \times 10^{-3} \text{ s}^{-1}$.

To better correlate the obtained TOF values with Pt particle size in the catalysts, plots of TOFs versus Pt particle size were made and shown in Fig. 7. Regressions of the TOF_a values (at 40 °C) and Pt particle sizes result in the following equations: $\text{TOF}_a = 0.027 \times 10^{-3} d^{-0.86}$. The changes of TOF_a with Pt particle size suggests that the reaction over these catalysts are structure-sensitive. This observation is inconsistent with the previous findings that either the TOFs are independent of particle size [40,41] or the TOF increases with Pt particle size [39]. Concerning the TOF_b, it is found that the dependence of TOF_b on the Pt particle size is completely different from that of TOF_a. The TOF_b values are almost constant with the changing Pt particle size (except for the 0.3Pt/TiO₂ catalyst).

The correlation between Pt particle size and TOFs has been similarly established on Au/TiO_2 catalysts for low temperature CO oxidation, in which TOF values based on Au dispersion (TOF_a)

Table 1Summary of catalytic results for CO oxidation over Pt/TiO₂ catalysts at 40 °C.

Catalyst	Pt particle size (nm)	CO conversion (%)	TOF _a (x10 ⁻³ s ⁻¹)	TOF _b (x10 ⁻³ s ⁻¹)
0.3Pt/TiO ₂ (0.1 g)	1.1	11.0	21.5	12.8
0.5Pt/TiO ₂ (0.05 g)	1.7	5.2	17.9	15.5
1.0Pt/TiO ₂ (0.05 g)	2.7	4.4	12.2	17.1
2.0Pt/TiO ₂ (0.05 g)	3.5	5.3	9.5	17.3
5.0Pt/TiO ₂ (0.1 g)	5.4	12.9	6.8	17.8
10Pt/TiO ₂ (0.1 g)	10.0	6.2	3.2	16.5

Table 2Summary of kinetic results of CO oxidation over 2.0Pt/TiO₂ catalyst at 40 °C.

Partial pressure (kPa)		CO conversion ^a (%)	Reaction rate (x10 ⁻⁷ mol g ⁻¹ s ⁻¹)
CO	O ₂		
1.0133	0.304	5.1	1.52
1.0133	0.5066	5.6	1.67
1.0133	1.0133	6.3	1.88
1.0133	2.0265	6.9	2.05
1.0133	3.0398	8.1	2.41
0.304	1.0133	17.4	1.55
0.5066	1.0133	11.9	1.78
2.0265	1.0133	4.1	2.44
3.0398	1.0133	3.6	3.21

^a The weight of catalyst was 300 mg.

declined with increasing Au particle size [42,43] while TOF values based on Au atoms at the Au–TiO₂ interface remained constant [44]. More importantly, such correlation gives an implication of the active sites for CO oxidation. Haruta et al. [42] and Overbury et al. [43] found that the TOF values for CO oxidation over Au/TiO₂ catalysts varied as particle size d^{-1} and suggested that the reaction takes place at the Au–TiO₂ interface because the ratio of Au atoms located at the interfacial perimeter of a supported hemispherical cap with diameter d to the number of Au atoms on the surface of the cap varies as d^{-1} . Recently, Fujitani and Nakamura [44] concluded that Au atoms on the Au–TiO₂ interface could be the active sites for CO oxidation at low temperature (<300 K) due to the fact that the TOF value based on Au atoms located on Au atoms at the Au–TiO₂ interface (TOF_b) was constant regardless of Au particle size.

In the present work, the TOF_a values are found to be proportional to $d^{-0.86}$, and the TOF_b values are constant regardless of Pt particle size. Such finding implies that CO oxidation over the Pt/TiO₂ catalysts may follow similar pathways as in Au/TiO₂ catalysts, namely, the reaction take place at the Pt–TiO₂ interface.

3.3. Kinetic study of CO oxidation over 2.0Pt/TiO₂ catalyst

Kinetic study of CO oxidation was performed on the 2.0Pt/TiO₂ catalyst at 40 °C. Absence of mass and heat transfer limitation was verified by checking the Weisz–Prater criterion and Mears' criterion. And the reactions were carried out at differential mode with CO conversions typically less than 15%. Table 2 summarizes the kinetic results of CO oxidation over the 2.0Pt/TiO₂ catalyst at 40 °C. The dependences of partial pressures of CO and O₂ on the reaction rate are demonstrated in Fig. 8a and c. It is found that the reaction rate increases with partial pressures of CO and O₂ in the feedstock. After taking logarithm of these values (Fig. 8b and d), the reaction order of CO and O₂ could be calculated. Thus, the power rate expression is $r = 1.98 \times 10^{-7} P_{CO}^{0.29} P_{O_2}^{0.19}$.

Fig. 9 shows the Arrhenius plot and parity plot of CO oxidation over the 2.0Pt/TiO₂ catalyst. From Fig. 9a, the apparent activation energy was calculated to be 41.5 kJ mol⁻¹. This value is higher than those obtained over Pt/SiO₂ catalysts (13–22 kJ mol⁻¹ [39]), but is lower than those obtained on Pt/Al₂O₃ catalysts (80–90 kJ mol⁻¹ [25]; 65 kJ mol⁻¹ [45]). And the parity plot shows (Fig. 9b) that the experimental reaction rates are consistent with the calculated reaction rates according to the rate expression $r = 1.98 \times 10^{-7} P_{CO}^{0.29} P_{O_2}^{0.19}$, which indicates that the derivation of the rate expression is valid.

Based on the rate expression, elementary steps of CO oxidation over Pt/TiO₂ catalyst could be derived. Among various reaction models, Mars van-Krevelen model and Eley Rideal model could be excluded because the former would result in a rate equation with a reaction order of 0 on O₂ partial pressure, and the latter would result in a rate equation with a reaction order of 1 on O₂ partial pressure (see Supplementary Information), which are not consistent with the kinetic results in the present work. Also, since TiO₂ is a reducible support, participation of its lattice oxygen in the reaction must be concerned. DRIFT experiment was performed on the 2.0Pt/TiO₂ catalyst after it was exposed in CO at 40 °C and the results are shown in Fig. 10. It can be seen that at elevated temperatures, the intensities of the IR bands continuously declines due to the desorption of CO molecules from the catalyst surface. Meanwhile, a new band at 2300–2350 cm⁻¹ (Fig. 10 inset) assigned to gas phase

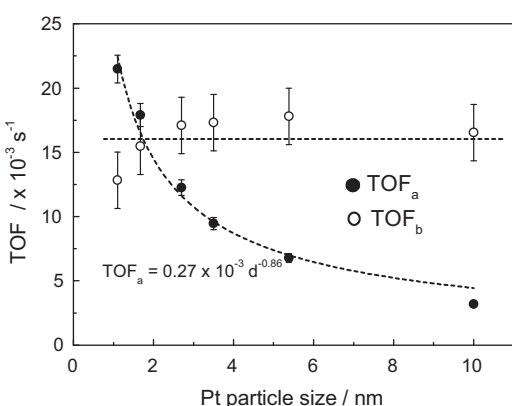


Fig. 7. TOFa and TOFb as a function of Pt particle size at 40 °C.

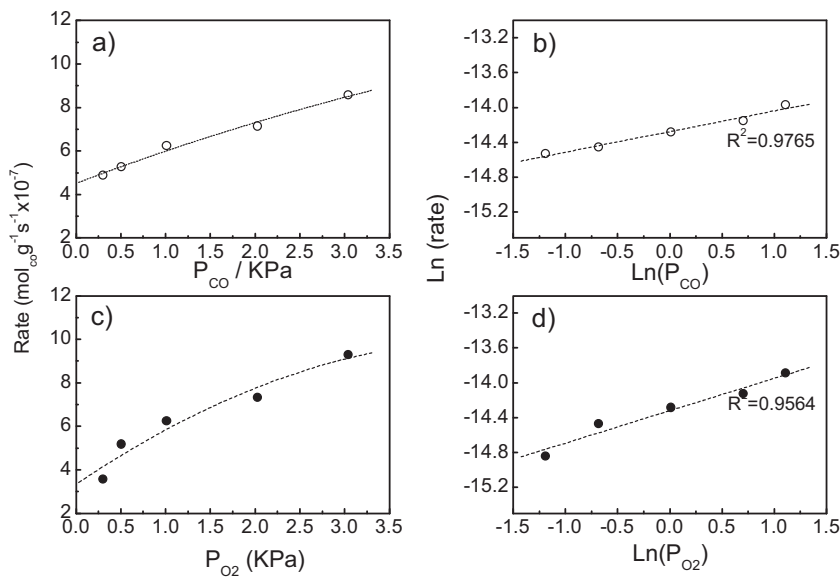


Fig. 8. Kinetic results of CO oxidation over 2.0Pt/TiO₂ at 40 °C.

CO₂ appears at 80 °C, indicating the formation of CO₂ by the reaction between CO and lattice oxygen. Note that the intensity of this band is extremely weak, it seems that the contribution of lattice oxygen in TiO₂ might be quite limited. However, these results (Fig. 10) are obtained in the absence of gas phase oxygen, if the gas phase oxygen could be continuously supplied as under reaction conditions, such contribution may also be significant.

Then we consider L-H models which were reported in literature. These models involving competitive adsorption and reaction of CO and O₂ on Pt surface (see Supplementary Information). According to these models, the derived rate expressions are $r = k_2[O_2]/(1 + K_1[CO])$ [19] and $r = k_3K_1K_2[O_2][CO]/(1 + K_1[CO])^2$ [25], which has a negative reaction order on CO partial pressure (−1 at near saturation of CO coverage). Thus these models are not

consistent with the kinetic results in the current work and should be excluded.

Besides, it was reported that CO oxidation could occur on Pt surface at relatively high temperature, which involves non-competitive adsorption of CO and O₂ on Pt surface atoms. For example, Gracia et al. reported CO oxidation over a Pt/SiO₂ catalyst at 100 °C [39]. Thus, elementary steps concerning surface reaction on Pt atoms could be derived as follows:

Reaction on Pt surface, non-competitive adsorption of CO and O₂.

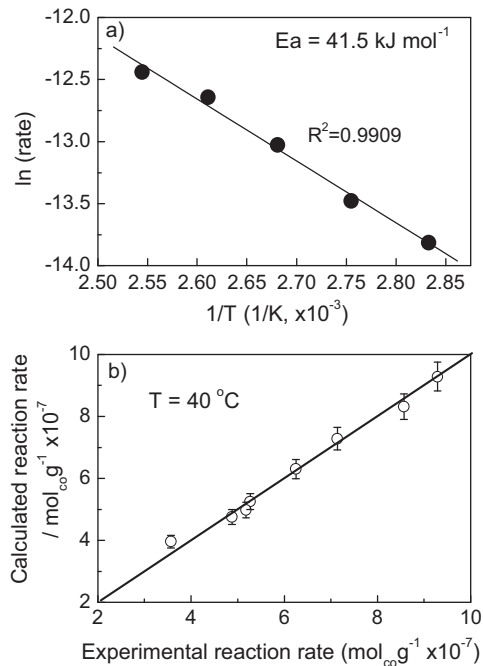
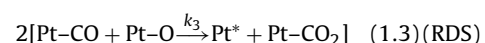
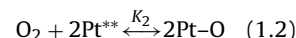
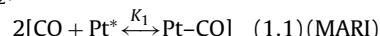


Fig. 9. (a) Arrhenius plot and (b) parity plot of CO oxidation over 2.0Pt/TiO₂ catalyst.

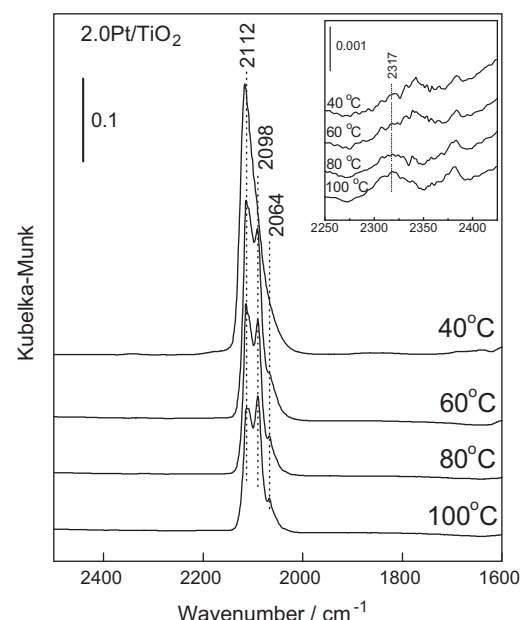


Fig. 10. DRIFT spectra of CO chemisorption at elevated temperatures after 2.0Pt/TiO₂ being exposed in CO at 40 °C.

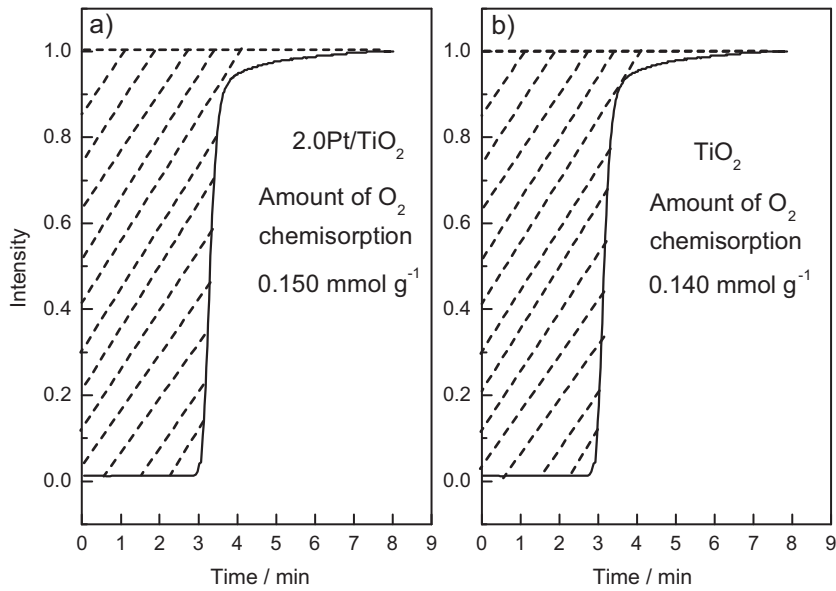
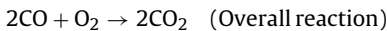
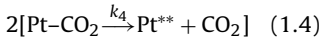


Fig. 11. O₂ chemisorption on 2.0Pt/TiO₂ and TiO₂ at 40 °C.



where Pt* and Pt** refer to different sites on surface Pt atoms.

With these elementary steps (1.1)–(1.4), the reaction rate expression is:

$$r = \frac{k_3 K_1 K_2^{1/2} [\text{CO}][\text{O}_2]^{1/2}}{(1 + K_1[\text{CO}]) (1 + K_2^{1/2} [\text{O}_2]^{1/2})}$$

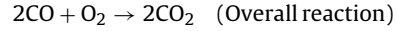
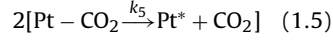
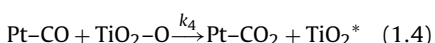
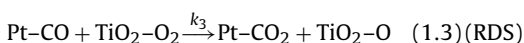
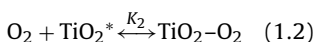
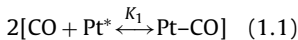
The rate equation is consistent with the kinetic results. However, concerning the fact that a reference 2.0Pt/SiO₂ catalyst is not active until the reaction temperature reaches 200 °C (Fig. 6), it is not likely that CO and O₂ could react on the surface Pt atoms at low temperature (40 °C). Therefore, this reaction model also could be excluded.

Considering the fact that CO oxidation may take place at the Pt–TiO₂ interface (Section 3.1), two models which involve CO chemisorption on Pt surface and O₂ chemisorption on TiO₂ are proposed.

Detailed elementary steps are as follows:

SET 1

Reaction on Pt–TiO₂ interface, with CO chemisorbed on Pt and O₂ chemisorbed on TiO₂. O₂ chemisorption is non-dissociative.

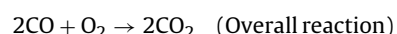
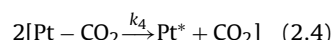
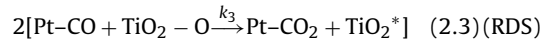
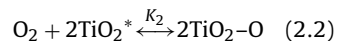
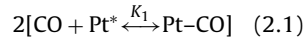


With these elementary steps (1.1)–(1.5), the reaction rate expression is:

$$r_1 = \frac{k_3 K_1 K_2 [\text{CO}][\text{O}_2]}{(1 + K_1[\text{CO}]) (1 + K_2[\text{O}_2])} \quad (1')$$

SET 2

Reaction on Pt–TiO₂ interface, with CO chemisorbed on Pt and O₂ chemisorbed on TiO₂. O₂ chemisorption is dissociative.



with these elementary steps (2.1)–(2.4), the reaction rate expression is:

$$r_2 = \frac{k_3 K_1 K_2^{1/2} [\text{CO}][\text{O}_2]^{1/2}}{(1 + K_1[\text{CO}]) (1 + K_2^{1/2} [\text{O}_2]^{1/2})} \quad (2')$$

In these two sets of elementary steps, the reaction between CO and oxygen species (either molecular O₂ or atomic O) is taken to be the rate determining step (RDS) (Eqs. (1.3) and (2.3)) and the chemisorption of either CO or O₂ is equilibrium. This is because if the CO or O₂ chemisorption is considered as the RDS, the reaction rate expression would contain reaction order of 1 on CO or O₂ partial pressure, which is not consistent with the obtained reaction orders of CO and O₂ in the power rate law equations between 0 and 1.

The chemisorption of CO on Pt surface is verified by the IR results (Fig. 5) and the chemisorption of O₂ on TiO₂ is verified by the O₂ chemisorption results shown in Fig. 11. The amount of chemisorbed O₂ was calculated by integrating the shadowed area. It can be seen that both the 2.0Pt/TiO₂ catalyst and TiO₂ support can chemisorb O₂, with the amount of chemisorbed O₂ slightly higher on the 2.0Pt/TiO₂ catalyst (0.150 mmol g⁻¹).

Both the reaction rate expressions (Eqs. (1) and (2)) fit well with the obtained kinetic results, because these two equations are equivalent to power rate law expression $r = k_a P_{CO}^n P_{O_2}^m$, where n and m are in the range of 0–1. However, in the present work, we could not distinguish whether the active oxygen species are molecular or atomic. Controversial conclusions also exist in Au/TiO₂ catalysts for CO oxidation [46].

One important issue that deserves consideration is the activation of oxygen on the catalyst. Although chemisorption of O₂ is confirmed (Fig. 11), no concrete evidence of activation of O₂ (either molecularly or atomically) on TiO₂ is provided in this work. Nevertheless, it is generally accepted that in Au catalysts supported on reducible oxides such as TiO₂, Fe₂O₃ and CeO₂, oxygen molecules may adsorb on the oxygen vacancies located on the support surface and consequently generate active oxygen species such as O₂[−] [47]. Another issue is the moisture effect on CO oxidation. Vital role of moisture in CO oxidation over supported Au catalysts has been extensively investigated, which could help in the activation of oxygen and the decomposition of carbonate [48]. Unfortunately, in the present work, precise concentration of moisture in the feedstock could not be measured; however, the role of moisture in CO oxidation over the Pt/TiO₂ catalyst might be also significant, which is similar to the cases of the Au/TiO₂ catalysts. Thus, CO oxidation over Pt/TiO₂ catalysts in the current work takes place at the Pt–TiO₂ interface at low reaction temperature. The CO molecules adsorb on Pt while the O₂ molecules (either molecular or atomic) adsorb on TiO₂, and the two reactants can migrate to interface position and react. This reaction model is similar to the findings in Au/TiO₂ catalyst for CO oxidation, in which the authors found that the reaction order on O₂ was 0.4 between 310 and 360 K, while that on CO was 0.2–0.6 and the activity of the catalyst could be attributed to a synergistic interaction between Au and TiO₂ [49]. This reaction model was recently confirmed by the findings of Maeda et al. [50], in which they performed *in situ* electrical conductance measurement and suggested that the oxygen molecules could be activated on the oxygen vacancies at Au–TiO₂ interface.

4. Conclusion

In this work, kinetic study of CO oxidation was performed over Pt/TiO₂ catalysts at low temperature. Regarding the Pt particle size effect, it was found that TOF based on Pt dispersion varied as a function of $d^{-0.86}$, while TOF based on Pt located at the periphery of Pt–TiO₂ interface remained constant, implying that those interfacial Pt atoms are the active sites for CO oxidation. Kinetic study of CO oxidation resulted in a rate expression of $r = 1.98 \times 10^{-7} P_{CO}^{0.29} P_{O_2}^{0.19}$, and elementary steps were proposed, which involved chemisorption of CO on surface Pt atoms

and O₂ chemisorption on TiO₂, and reaction between these two species.

Acknowledgments

This work is financially supported by Natural Science Foundation of China (Grant No. 21173195 and 21203167).

Appendix A. Supplementary data

Supplementary data associated with this article can be found, in the online version, at <http://dx.doi.org/10.1016/j.apcatb.2013.05.068>.

References

- [1] D.R. Schryer, B.T. Upchurch, B.D. Sidney, K.G. Brown, G.B. Hoflund, R.K. Herz, *J. Catal.* 130 (1991) 314–317.
- [2] Y.Z. Yuan, A.P. Kozlova, K. Asakura, H.L. Wan, K. Tsai, Y. Iwasawa, *J. Catal.* 170 (1997) 191–199.
- [3] M. Haruta, T. Kobayashi, H. Sano, N. Yamada, *N. Chem. Lett.* 16 (1987) 405–408.
- [4] M. Haruta, S. Tsubota, T. Kobayashi, H. Kageyama, M.J. Genet, B. Delmon, *J. Catal.* 144 (1993) 175–192.
- [5] S.M. McClure, D.W. Goodman, *Chem. Phys. Lett.* 469 (2009) 1–13.
- [6] D.R. Schryer, B.T. Upchurch, B.D. Sidney, K.G. Brown, G.B. Hoflund, R.K. Herz, *J. Catal.* 130 (1991) 314–317.
- [7] D.R. Schryer, B.T. Upchurch, J.D. Van Norman, K.G. Brown, J. Schryer, *J. Catal.* 122 (1990) 193–197.
- [8] M. Fernández-García, A. Martínez-Arias, L.N. Salamanca, J.M. Coronado, J.A. Anderson, J.C. Conesa, J. Soria, *J. Catal.* 187 (1999) 474–485.
- [9] M.F. Luo, J.M. Ma, J.Q. Lu, Y.P. Song, Y.J. Wang, *J. Catal.* 246 (2007) 52–59.
- [10] M.F. Luo, Y.P. Song, J.Q. Lu, X.Y. Wang, Z.Y. Pu, *J. Phys. Chem. C* 111 (2007) 12686–12692.
- [11] K. Dadir, S.H. Kim, S.M. Kim, H. Ha, J.Y. Park, *J. Phys. Chem. C* 116 (2012) 24054–24059.
- [12] L. Liu, F. Zhou, L. Wang, X. Qi, F. Shi, Y. Deng, *J. Catal.* 274 (2010) 1–10.
- [13] M. Che, C.O. Bennett, *Adv. Catal.* 36 (1989) 55–172.
- [14] F.J. Gracia, J.T. Miller, A.J. Kroft, E.E. Wolf, *J. Catal.* 209 (2002) 341–354.
- [15] S.T. Daijels, A.R. Overweg, M. Makkee, J.A. Mouljin, *J. Catal.* 230 (2005) 52–65.
- [16] A.P. Jia, S.Y. Jiang, J.Q. Lu, M.F. Luo, *J. Phys. Chem. C* 114 (2010) 21605–21610.
- [17] R.H. venderbosch, W. Prins, W.P.M. Van Swaaij, *Chem. Eng. Sci.* 53 (1998) 3355–3366.
- [18] P.J. Berlowitz, C.H.F. Peden, D.W. Goodman, *J. Chem. Phys.* 92 (1988) 5213.
- [19] G. Djéga-Mariadassou, M. Boudart, *J. Catal.* 216 (2003) 89–97.
- [20] R.H. Nibbelke, M.A.J. Campman, J.H.B.J. Hoebink, G.B. Marin, *J. Catal.* 171 (1997) 358–373.
- [21] M.P. Harold, M.E. Garske, *J. Catal.* 127 (1991) 524–552.
- [22] A. Bielanski, J. Haber, *Oxygen in Catalysis*, Dekker, New York, 1991, pp. P211.
- [23] G.I. Golodets, J.R.H. Ross, *Heterogenous Catalysis Reactions involving Molecular Oxygen, Studies in Surface Science and Catalysis*, vol. 15, Elsevier, Amsterdam, 1983, pp. P280.
- [24] T. Matsushima, *Surf. Sci.* 79 (1979) 63–75.
- [25] A.D. Allian, K. Takanabe, K.L. Fujdala, X. Hao, T.J. Truex, J. Cai, C. Buda, M. Neurack, E. Iglesia, *J. Am. Chem. Soc.* 133 (2011) 4498–4517.
- [26] M. Kotobuki, R. Leppelt, D.A. Hansgen, D.W. Behm, *J. Catal.* 264 (2009) 67–76.
- [27] D. Widmann, R.J. Behm, *Angew. Chem. Int. Ed.* 50 (2011) 10241–10245.
- [28] H.S. Fogler, *Elements of Chemical Reaction Engineering*, 4th edition, Pearson Education Inc., 2006, pp. 839.
- [29] M. Shacham, M.B. Cutlip, M. Elly. Polymath, Copyright 2006. <http://www.polymath-software.com>
- [30] J. Silvestre-Albero, J.C. Serrano-Ruiz, A. Sepúlveda-Escribano, F. Rodríguez-Reinoso, *Appl. Catal. A: Gen.* 292 (2005) 244–251.
- [31] A.M. Ruppert, T. Paryjcak, *Appl. Catal. A: Gen.* 320 (2007) 80–90.
- [32] J. Silvestre-Albero, A. Sepúlveda-Escribano, F. Rodríguez-Reinoso, A.J. Anderson, *J. Catal.* 223 (2004) 179–190.
- [33] P. Reyes, G. Pecchi, M. Morales, J.L.G. Fierro, *Appl. Catal. A: Gen.* 163 (1997) 145–152.
- [34] A. Franciso, R. Paola, R.R. Franciso, *J. Catal.* 260 (2008) 113–118.
- [35] C.H. Lin, J.H. Chao, C.H. Liu, J.C. Chang, F.C. Wang, *Langmuir* 27 (2008) 9907–9915.
- [36] O.S. Alexeev, S.Y. Chin, M.H. Engelhard, L. Ortiz-Soto, M.D. Amiridis, *J. Phys. Chem. B* 109 (2005) 23430–23443.
- [37] P. Panagiotopoulou, A. Christodoulakis, D.I. Kondarides, S. Boghosian, *J. Catal.* 240 (2006) 114–125.
- [38] P.A. Carlsson, L. Österlund, P. Thormählen, A. Palmqvist, E. Fridell, J. Jansson, M. Skoglundh, *J. Catal.* 226 (2004) 422–434.
- [39] F.J. Gracia, L. Bollmann, E.E. Wolf, J.T. Miller, A.J. Kropf, *J. Catal.* 220 (2003) 382–391.
- [40] N.W. Cant, *J. Catal.* 62 (1980) 173–175.
- [41] D.R. Rainer, M. Koranne, S.M. Vesccky, D.W. Goodman, *J. Phys. Chem. B* 101 (1997) 10769–10774.

[42] M. Haruta, S. Tsubota, T. Kobayashi, H. Kageyama, M.J. Genet, B. Delmon, *J. Catal.* 144 (1993) 175–192.

[43] S.H. Overbury, V. Schwartz, D.R. Mullins, W. Yan, S. Dai, *J. Catal.* 241 (2006) 56–65.

[44] T. Fujitani, I. Nakamura, *Angew. Chem. Int. Ed.* 50 (2011) 10144–10147.

[45] A. Bourane, D. Bianchi, *J. Catal.* 202 (2001) 34–44.

[46] B. Grzybowska-Świerkosz, *Catal. Today* 112 (2006) 3–7.

[47] G.C. Bond, C. Louis, D.T. Thompson, *Catalysis by Gold*, Imperial College Press, 2006, pp. 194–195.

[48] M. Daté, M. Okumura, S. Tsubota, M. Haruta, *Angew. Chem. Int. Ed.* 43 (2004) 2129–2132.

[49] S.D. Lin, M. Bollinger, M.A. Vannice, *Catal. Lett.* 17 (1993) 245–262.

[50] Y. Maeda, Y. Iizuka, M. Kohyama, *J. Am. Chem. Soc.* 135 (2013) 906–909.